Materials Chemistry and Physics 121 (2010) 541–548

Contents lists available at ScienceDirect

Materials Chemistry and Physics

journal homepage: www.elsevier.com/locate/matchemphys

Capillary-driven assembly of ZnO nanowire arrays into micropatterns

Yang Tang[a,b], Dongxu Zhao[a,*], Jie Chen[c], Nelia Wanderka[c], Dezhen Shen[a], Fang Fang[a,b], Zhen Guo[a,b], Jiying Zhang[a], Xiaohua Wang[d]

[a] Key Laboratory of Excited State Processes, Changchun Institute of Optics, Fine Mechanics and Physics, Chinese Academy of Sciences, 16 East Nan-Hu Road, Open Economic Zone, Changchun 130033, People's Republic of China
[b] Graduate School of the Chinese Academy of Sciences, People's Republic of China
[c] Helmholtz-Zentrum Berlin für Materialien und Energie GmbH, Hahn-Meitner Platz 1, 14109 Berlin, Germany
[d] National Key Laboratory of High Power Semiconductor Laser, Changchun University of Science and Technology, 7089-WeiXing Road, ChangChun 130022, People's Republic of China

ARTICLE INFO

Article history:
Received 8 April 2009
Received in revised form 18 January 2010
Accepted 13 February 2010

Keywords:
Nanostructures
Vapor deposition
Evaporation
Adhesion

ABSTRACT

The vertically aligned ZnO nanowire arrays prepared by vapor transport process can be assembled into complex micropatterns under capillary force. The deflection of the flexible ceramic nanowire is closely related to the liquid tension coefficient, mechanical and structural properties of the ZnO nanowires. The bended nanowires are adhesive together because the solid adhesion energy is sufficient to withstand the restoring elastic force of the deformed nanowires. The size of the bundling pattern can be controlled by varying the aspect ratio of the nanowire. The deflection of the ZnO nanostructure composed of a nanowire and a base is multifarious.

1. Introduction

The arrays of nanostructures like carbon nanotubes (CNTs) or silicon nanowires (NWs) have potential applications in fields of biomedicine, chemistry, physics and materials. It has been observed that the separated nanotubes or nanowires could be bundled together during their treatments by immersion in water or by the spread of a water droplet. The bundling process or self-assembly process is an efficient and preferred approach to build nanostructure arrays into ordered micro- and macroscopic structures. The process of self-assembly of arrays was intensively investigated in the recent years. There are two ways for the production of self-assembled patterns of nanotubes. Whereas some studies have been reported about the CNTs that self-assembly bundle together to form a cellular network structure by immersion into a liquid and dried [1–6] while the other studies discovered that this self-assembly process took place during the spreading of a liquid droplet [7,8]. Nguyen et al. found that the aligned CNTs collapsed and formed a pyramid-like after the oxidative treatment by using the carboxylic acid solution [1]. Lau et al. verified that the vertically aligned CNT forests, after exposure to water, bundled together as a result of the attractive capillary forces arose during evaporative drying [2]. It was reported by Chakrapani et al. that capillary forces arising during the evaporation of liquids from dense CNT arrays were used to reassemble the nanotubes into two-dimensional contiguous cellular foams [3]. Jiang et al. also observed the cellular network formation on long CNT arrays [7]. Yan et al. found that large-scale pyramid-like micropatterns were prepared by capillary-driven assembly during the evaporation of water from aligned CNTs [4]. The same phenomenon was also found on silicon nanowires (NWs). Zhao et al. reported that the vertically aligned silicon nanorod array would deform into bundling patterns by the spread of a water droplet [8]. The stability and the dynamics of bundled Si nanorod arrays were also studied [9,10]. They named the bundling phenomenon as the "nanocarpet effect" [8]. The "nanocarpet effect" is defined as that the bundling of vertically aligned nanostructure array will happen owing to the capillary force when the liquid touches the surface of the arrays. However, the happen of the "nanocarpet effect" is closely related to the arrangement of the nanowire or nanorod arrays, the Young's modulus, the aspect ratio and the surface tension of the liquid [11].

As a wide band-gap semiconductor, ZnO one-dimensional nanostructures have applications as ultraviolet lasers [12], field-effect transistors [13], gas sensors [14], field-emission displays [15], and nanogenerators [16,17]. Some investigations on elastic properties of ceramic ZnO NWs have been reported [18–20]. The atomic force microscopy (AFM) manipulation of the ZnO nanorings, nanobows and NWs demonstrated their mechanical toughness and flexibility [21,22]. When the external force was removed, the NWs would turn back to the original position. But if the applied force

* Corresponding author. Tel.: +86 431 86176322; fax: +86 431 84627031.
E-mail address: dxzhao2000@yahoo.com.cn (D. Zhao).

0254-0584/$ – see front matter © 2010 Elsevier B.V. All rights reserved.
doi:10.1016/j.matchemphys.2010.02.018

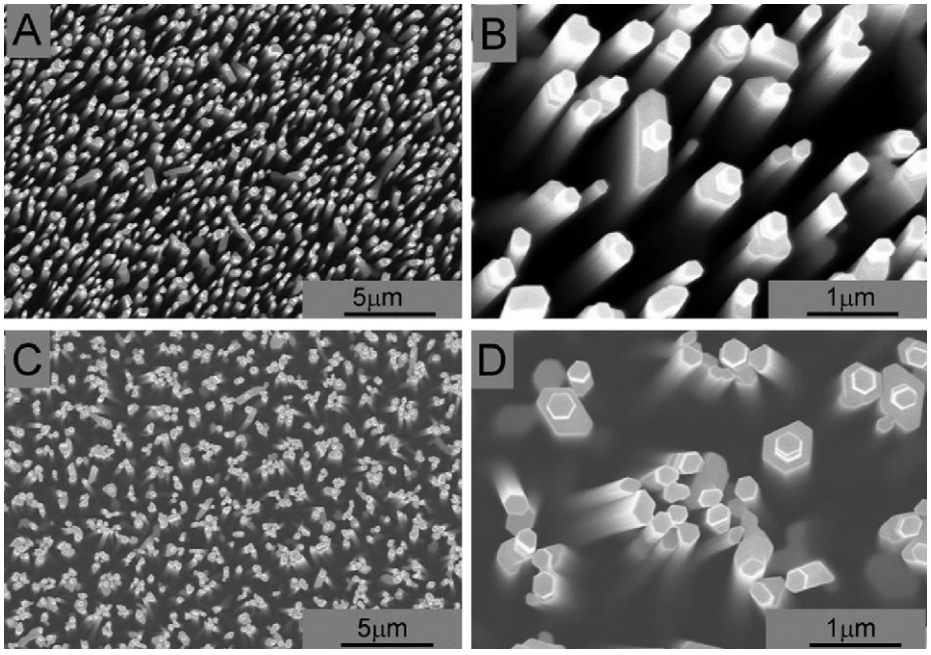

Fig. 1. (A) and (B) The vertically aligned ZnO NW arrays on silicon substrate before immersion into the deionized water. (C) and (D) The bundling pattern of ZnO NW arrays after immersion into water and evaporation at room temperature.

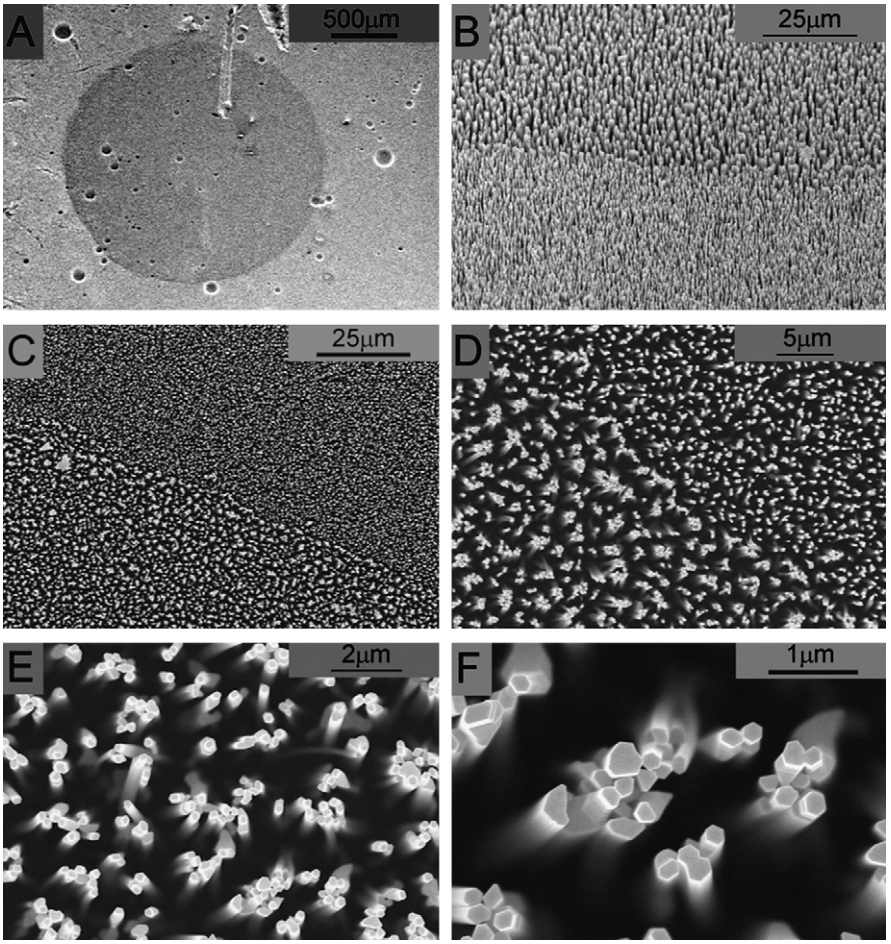

Fig. 2. (A) The circular mark of the bundling ZnO NW arrays after dripping a droplet (0.001 mL) on the surface of the vertically aligned NW arrays and evaporation at room temperature. (B–D) The boundary between the bundling ZnO NWs and the unbundling nanowires. (E) and (F) The bundling ZnO NW arrays in the circular mark. A top view is for (C)–(F) images and a tilted view (20°) is for (A) and (B) images.

exceeded a limit value, ZnO NW would be fractured. As a ceramic material, the exceptional flexibility for ZnO NWs can be confirmed but there is no residual plastic deformation. The bundling pattern of ZnO NW arrays have been reported in a hydrothermal method after the sample put out [23–27].

In this paper, we demonstrate that a large bending of the flexible ceramic ZnO NWs could be produced by capillary force of water. As a result of the sufficient adhesion energy of the solid–solid contact, the NWs assembled into micropatterns. The deformation of the NW is strongly dependent on the aspect ratio, the arrangement of NW array and the morphology of the NW, which lead to assembly into complex micropatterns.

2. Experimental methods

Our study was based on the aligned ZnO NWs arrays grown on p-Si (1 0 0) substrate by vapor transport process. The silicon substrate was pre-coated with a ZnO thin layer. The details of the NW growth have been described also in paper [28,29]. The process of assembling the ZnO NWs into micropatterns was carried out using two methods. One method was to immerse the as-grown ZnO NWs into the deionized water (18.23 MΩ cm), then taken out and dried at room temperature (~298 K). The other method was to drip a droplet of deionized water (0.001 mL) on the surface of the vertically aligned ZnO NW arrays and then dried at the room temperature. The morphology and microstructure of all the NWs were observed by field-emission scanning electron microscopy (FESEM, Hitachi S-4800). Thin-foil specimens suitable for high-resolution transmission electron microscope (HRTEM) observations were prepared by mechanical thinning up to 20 μm thick followed by Ar ion milling. The microstructure of samples was characterized by TEM in a Philips CM30 operated at 300 kV.

3. Results and discussion

Fig. 1A and B shows SEM images of well-aligned ZnO NWs with hexagonal morphology of the wires in the cross-section. The nanowires are ~200 nm in diameter and ~10 μm in length. They

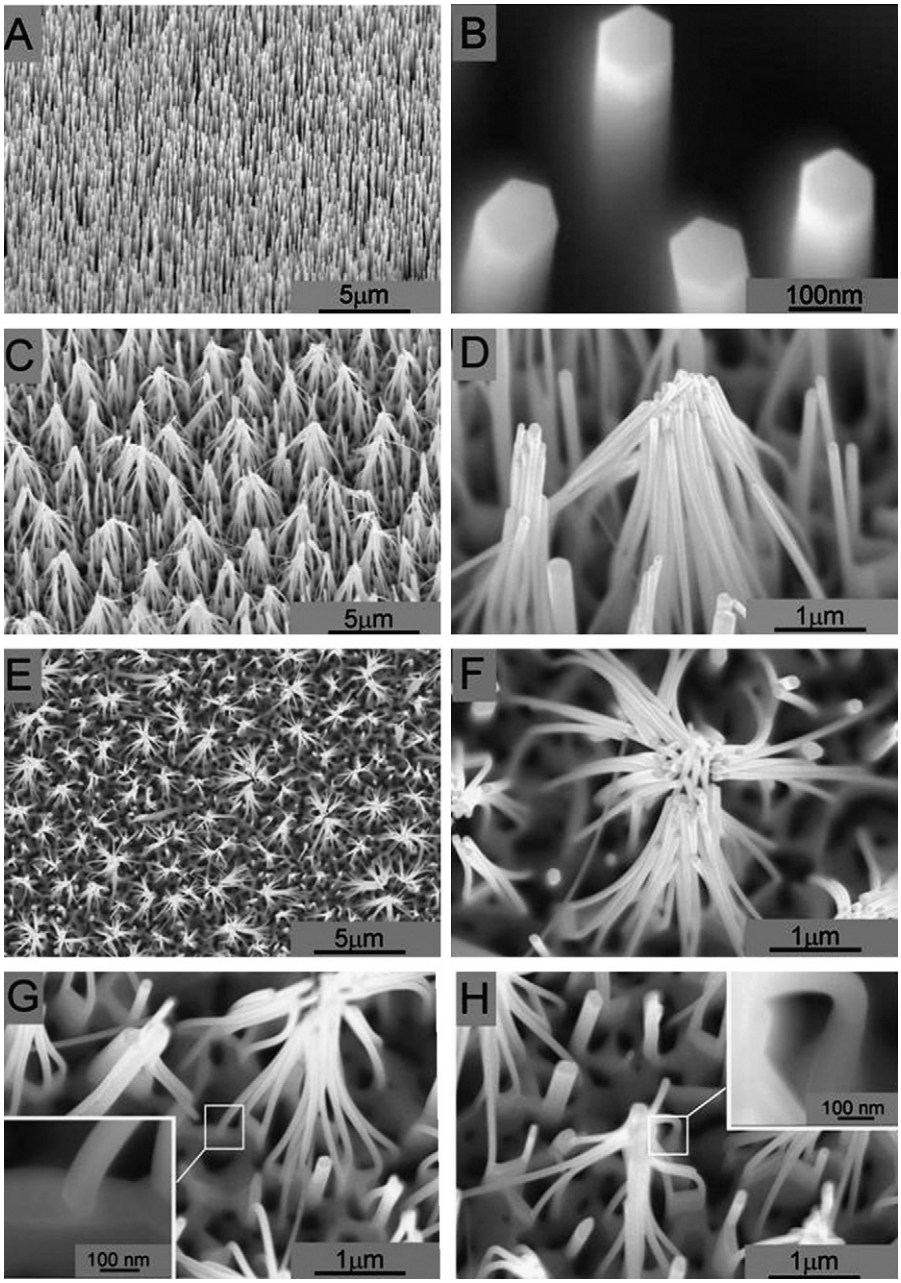

Fig. 3. (A) and (B) The vertically aligned ZnO NW arrays with the diameter of 100 nm and the length of 6 μm (the aspect ratio is 60) grown on silicon substrate are from the tilted view (20°). (C)–(F) The bundling ZnO NW arrays after immersion into the deionized water and evaporation at room temperature. A tilted view (20°) is for (C) and (D) and a top view is for (E) and (F). (G) and (H) The roots of bundling ZnO NWs. The inset of (G) and (H) shows enlarged views of the bended ZnO NWs.

are grown perpendicularly on the substrate. The NWs are straight and have no bending or interconnection between them. Fig. 1C and D shows ZnO NWs after immersion in water and drying at room temperature. The previously vertical aligned NW arrays are bended together and formed NW clusters. The tips of the bending NWs were firmly adhered together. The bending and adhesion of NWs happened during the evaporation of the water, as a result of the large capillary force and adhesion energy. The NW clusters are stable even after a long storing time (2 months) or after annealing the sample for 1 h at 700 °C in air, no obvious change of morphology could be obtained.

The ZnO NWs were also treated using dropped deionizer water. SEM image in Fig. 2A shows a conspicuous circular mark in diameter of ~1.9 mm on the surface of the NWs where the droplet was dropped. As can be seen in Fig. 2B–D there are significant differences of the morphology for the NWs inside and outside the circle. The morphology of NWs in the droplet-untouched region was straight and vertically aligned. In contrast, the NW arrays transform into the bundling pattern in the droplet-touched region. The bundling process of NWs by this method is due to the hydrophobic property of ZnO NWs grown by vapor transport [30]. Because there is no water spreading through the spatial of hydrophobic ZnO NWs and therefore there is not to expect an asymmetry distribution of capillary force during the water invasion. Consequently, the morphology of the bundling patterns does not change obviously with the distance from the center of the circle mark. The bundling of NWs using the second method (Fig. 2E and F) is similar to the pattern of the NW clusters immersed into water (Fig. 1). Therefore, all further experiments with NWs were carried out by immersion into water only.

The self-assembly process of the ZnO NW arrays into micropatterns can be described into two parts: (a) the bending of NWs and (b) the adhesion. The driving force of the NW bending is attributed to the capillary interaction between the neighboring NWs. Mechanical bending of the NWs acts as counterforce to balance the capillary force [11]. The surface-tension induced differences between the pressures of air and liquid is especially large owing to the narrow spacing between NWs (hundreds of nanometers). The pressure difference exerts a bending moment on the NWs. These large deformations are possible because of the extraordinary flexibility of ZnO NWs [22]. The bended NWs are adhered together because the solid adhesion energy is sufficient to withstand the restoring elastic force of the deformed NWs. Mastrangelo and Hsu have theoretically studied the mechanical collapse and adhesion of microstructures under capillary forces [31,32]. They introduced two quantities N_{EC} and N_P called elastocapillary number and peel number, respectively. If the N_{EC} and N_P <1 the cantilever is free and when the N_{EC} and N_P >1 it is pinned to the substrate. Assuming that there are two ZnO NWs which have the cross-rectangle section, one is stable and the other bends towards it under capillary force. The two numbers are given by the following equations [31,32]:

$$N_{EC} = \frac{Ed^2D^3}{9\gamma_L \cos\theta_C l^4} \quad (1)$$

$$N_P = \frac{3Ed^2D^3}{8\gamma_S l^4} \quad (2)$$

where E is the Young modulus, d is the space between NWs, D is the NW diameter, l is the NW length, γ_L is the liquid surface tension, γ_S is the interfacial adhesion energy of per unit contact area and θ_C is the contact angle between NW and liquid. The critical length L_{EC} of bending and the critical L_P of adhesion are respectively [33]:

$$L_{EC} = \left(\frac{Ed^2D^3}{9\gamma_L \cos\theta_C}\right)^{1/4} \quad (3)$$

$$L_P = \left(\frac{3Ed^2D^3}{8\gamma_S}\right)^{1/4} \quad (4)$$

Thus, for the NWs if l (l is the length of NW) < L_{EC}, the NWs would not be bended by capillary and they would be bended when $l > L_{EC}$. Moreover, if $l < L_P$, the NWs would not be adhesive and they would be adhesive when $l > L_P$.

The formation of the micropatterns by the bending and condensation of NWs additionally depends on the liquid tension coefficient, structural properties of the ZnO NWs like their alignment, narrow spacing, high aspect ratios, flexibility and mechanical strength. Zhao et al. have studied the factors that determine the size

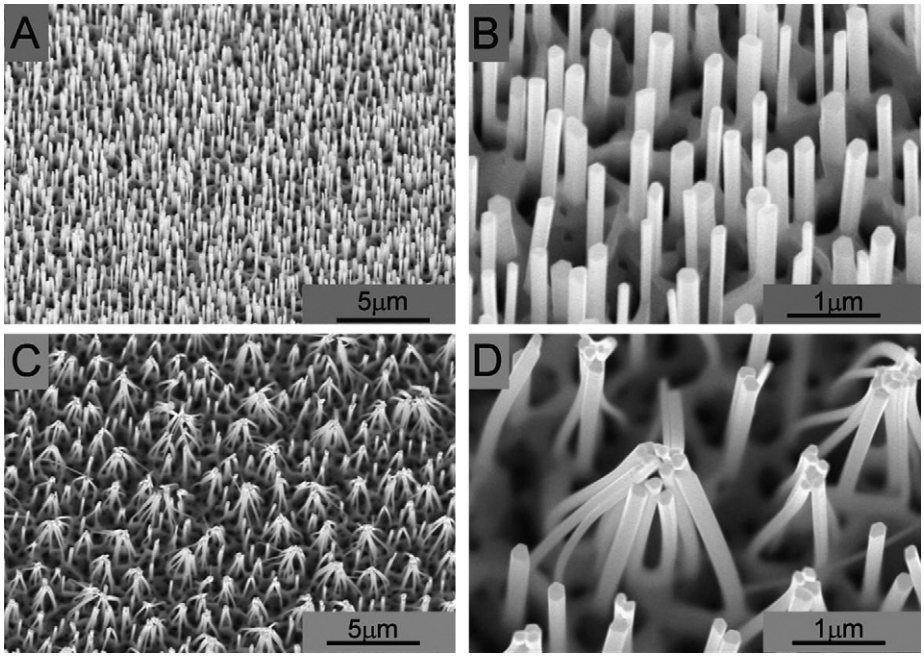

Fig. 4. (A) and (B) The vertically aligned ZnO NW arrays with the diameter of 200 nm and the length of 3.5 μm (the aspect ratio is 17.5) grown on silicon substrate. (C) and (D) The bundling ZnO NW arrays after immersion into the deionized water and then evaporation at room temperature.

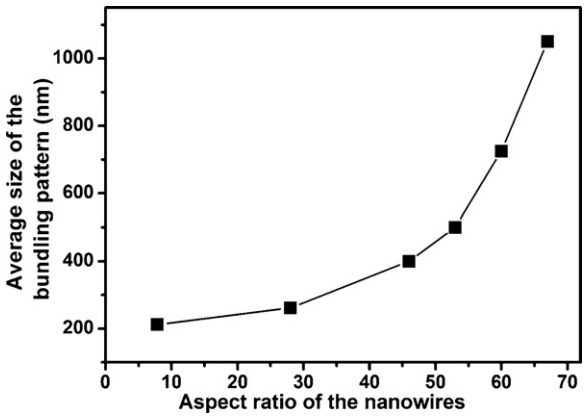

Fig. 5. The average size of the bundling patterns as a function of the aspect ratio of the NWs.

of the bundling cluster. They proposed a simple model based on the balance between mechanical bending and capillary interaction to investigate the cluster size in nanocarpet effect. The cluster energy minimization reveals the critical cluster size as follows [11].

$$N - 1 = \frac{-10\pi h^3 \gamma_L \cos^2\theta_C \ln(\gamma_e qs)}{D^2(d-D)^2 E} \quad (5)$$

The $\gamma_e = 1.781072418\ldots$, is called the Euler–Masceroni number. The $q = \Delta\rho g/\gamma$, characterizing the capillary length, where $\Delta\rho$ is the liquid density difference around the two rods, and g is the gravitational acceleration. The term s represents the separation of the menisus of the two rods. The equation can be expressed as follows.

$$N - 1 \propto \frac{r^3 D\sigma}{(1 - f^{1/2})^2} \quad (6)$$

where $r = l/D$ is the aspect ratio of the NWs, $f = \pi D^2/\pi d^2$ is the coverage of NWs on the surface, and $\sigma = 1/\pi d^2$ is the density of the NWs. It was noted that the higher the aspect ratio is, the larger the cluster size is. Based on the above analysis, we have synthesized two kinds of ZnO NWs with different aspect ratios in order to

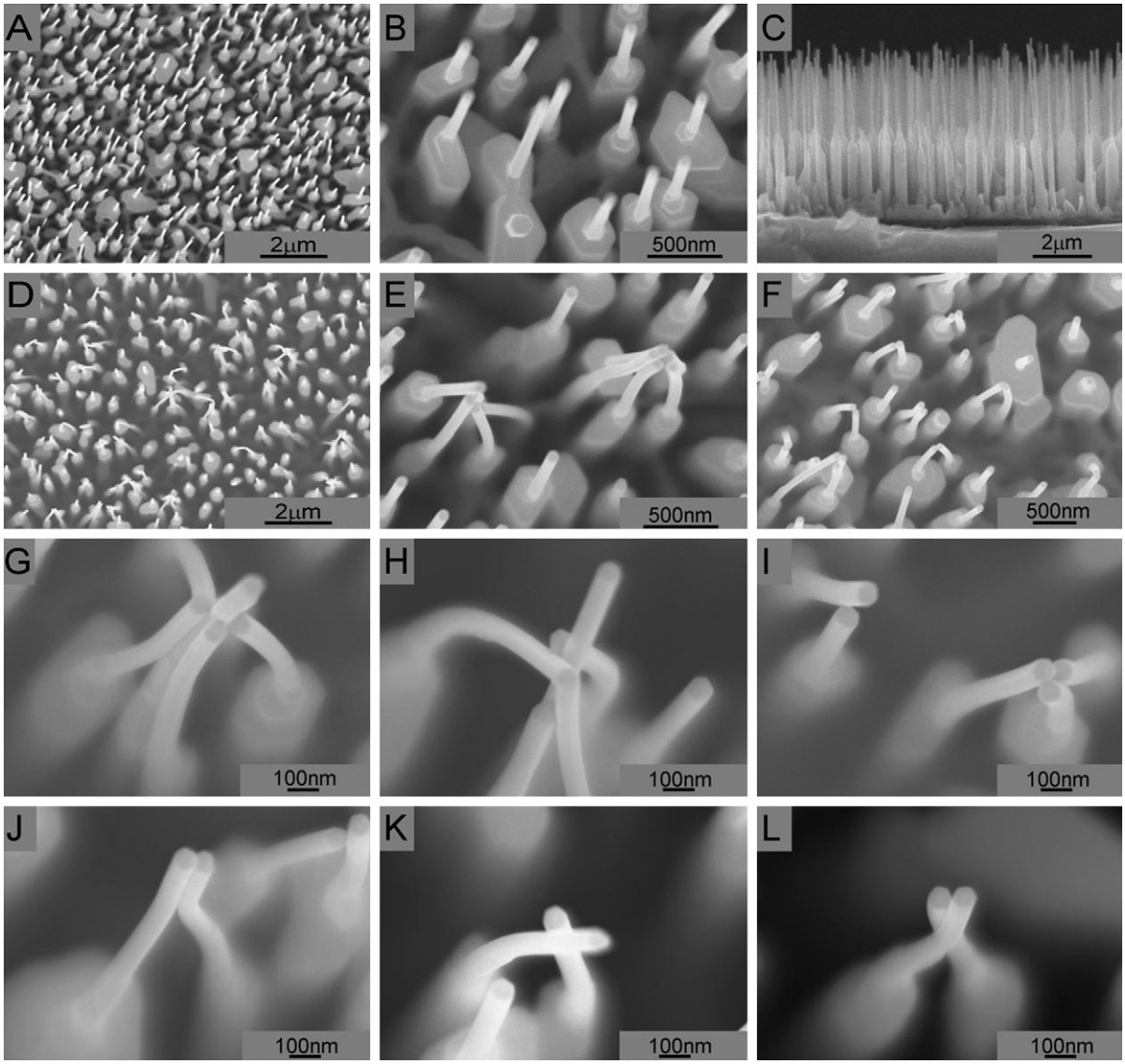

Fig. 6. (A) and (B) The vertically aligned ZnO NW arrays grown on silicon substrate. (C) A section view shows that the NW is composed of a base. The NW has the diameter of 100 nm and the length of 3 μm while the base has the length of 3 μm and the diameter ranging from 200 nm to 2 μm. (D)–(L) The bundling ZnO NWs are after immersion into the deionized water and evaporation at room temperature.

obtain bundling pattern with different cluster size. One type of the ZnO NW arrays has a diameter of 100 nm and a length of 6 μm (the aspect ratio is 60) as shown in Fig. 3A and B. The NWs are vertically aligned and straight. After immersion into deionized water there were obviously observed changes in the morphology. The NWs, which were straight before, become bended and the tips of the NWs were attached together as depicted in Fig. 3C–F. The originally erect NW arrays were transformed to the arrays of "microstacks", in which every group of some NWs were bending towards the center of the stacks. The images of Fig. 3D and F show that one stack might be consisted of a large number of bended NWs or several ones. Moreover, the stacked NWs tend to be adhesive. As can be seen from Fig. 3G the bending fraction of some NWs could appear at the root. Furthermore, some NWs could bend into almost orthogonal shape without breaking (Fig. 3H). It is certain that all the bending ZnO NWs kept their hexagonal shape. According to Eq. (6), the size of the bundling pattern depends on the aspect ratio of the NWs, the coverage of the NWs on the surface and the density of the NWs. For the NWs with certain aspect ratio, the larger the density of NWs is, the larger the pattern size is. The density distribution of the NWs in Fig. 3 is not exactly homogeneous. Therefore the inhomogeneous distribution of the NW density in local regions resulted in the uneven sizes of the bundling patterns. As shown in Fig. 3C and E, the ZnO NWs with the same aspect ratio can be assembled into different bundling pattern as well in some local regions. Excluding the impact of the aspect ratio, the density of the NWs and the coverage of the NWs on the surface are the main factors which influence the size of the patterns.

The other type of the ZnO NW arrays has a size: about 200 nm in diameter and about 3.5 μm in length (the aspect ratio is 17.5). The density of these NW arrays is similar to NW arrays having aspect ration of 60. The NWs are vertically aligned and straight (Fig. 4A and B) before immersion. After immersion into deionized water the vertically NW arrays are transformed into bundling patterns (Fig. 4C and D). It can be observed that the size of bundling cluster (Fig. 4D) is particularly smaller than that of the cluster shown in Fig. 3D owing to the different aspect ratios. Therefore, from these observations we can deduce that the size and the morphology of bundling pattern can be controlled by changing the aspect ratio of the ZnO NWs. The average size of the bundling patterns as a function of the aspect ratio of the NWs is plotted in Fig. 5. The course of the curvature indicates that the size of the bundling patterns became smaller with decreasing aspect ratio of the NWs.

The characterized morphology of the NW has a great impact on the bundling pattern. We have synthesized the unique morphological ZnO NWs grown on a base. The silicon as a substrate was pre-coated with a ZnO thin layer. The ZnO NWs in the length are composed of different sizes. The NW has the diameter of 100 nm and the length of 3 μm, while the base has the length of 3 μm and the diameter ranging from 200 nm to 2 μm (Fig. 6A–C). Fig. 6A–C shows the original morphologies of the ZnO nanostructure before immersion. The NWs and the base are straight and

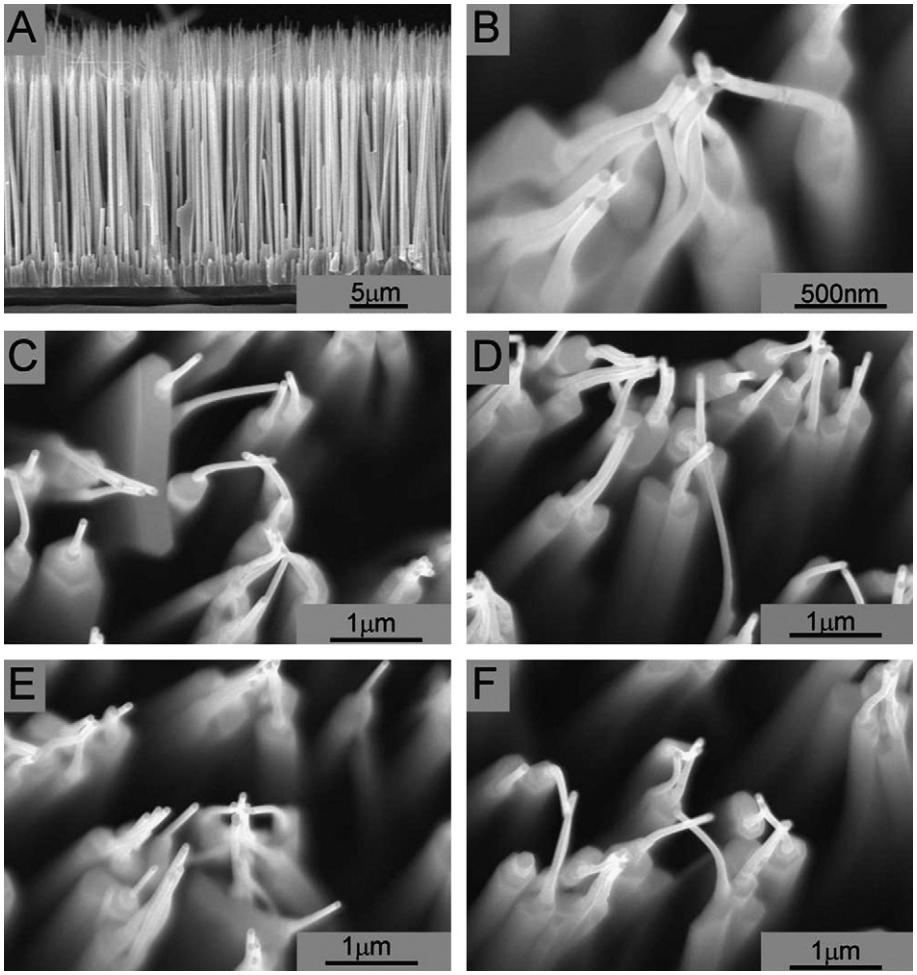

Fig. 7. (A) A section view shows that the nanowire is composed of a base. The base has the height of 20 μm and the diameter ranging from 200 nm to 2 μm. The nanowires grown on the base has the diameter of 100 nm and the length of 3 μm. (B)–(F) The bundling ZnO nanowires are shown after immersion into the deionized water and evaporation at room temperature.

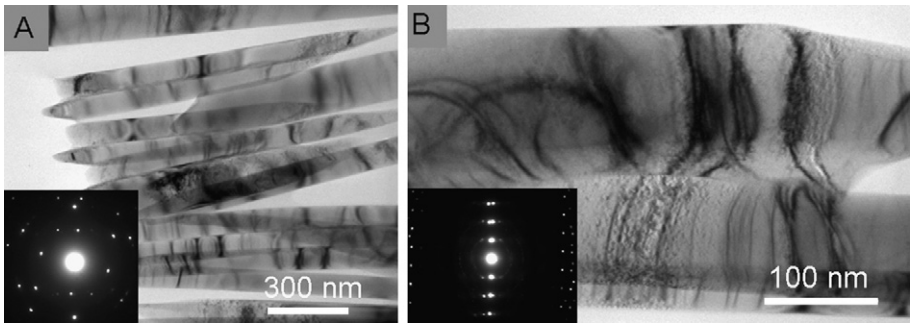

Fig. 8. Bright field TEM images of several touched NWs. The corresponding selected area electron diffraction patterns are in inset.

vertically aligned. From Fig. 6D–F can be observed that the deformation of NW after immersion in the water did not happen to every NW. Some NWs kept their original morphology while others were deformed drastically. Several NWs bent to be attached together (Fig. 6E and F). As we can see from Fig. 6G, five NWs bent towards the central NW which did not bent greatly. Furthermore, the NWs could bend more extraordinarily, which is imaged in Fig. 6H. Two or three NWs could bend to be attached together as shown in Fig. 6I. For two NWs actuated together, one could deform indistinctively while the other one exhibited enormous deformation (Fig. 6J). The capillary-driven multifarious pattern may be attributed to the asymmetric distribution of water among the NWs which is caused by unique morphology of the as-grown ZnO nanostructures. Especially the large range of the base part in size (0.2–2 μm) enhanced the asymmetric distribution of water during the drying process. Interestingly, the two NWs bending towards each other could form a cross (Fig. 6K) or be entangled with each other (Fig. 6L). The cross pattern of the two NWs indicated that the NWs bent to each other but the adhesive region existed on the middle parts rather than the upper parts of the NWs. The capillary-driven entangled pattern of the NWs (Fig. 6L) might be a further evolution of the cross pattern. Moreover, all the bending NWs did not appear to be broken and there is no change to the base part of the nanostructure. The capillary force did not deflect the base part, but the deformation would happen to the base with a larger aspect ratio. We also synthesized some ZnO nanostructures with a base of 20 μm in the length about 200 nm to 2 μm in diameter. The NW grown on the base has the diameter of 100 nm and the length of 3 μm (Fig. 7A). After immersion into the deionized water the different morphological changes of the nanostructure were observed. The bases of the unique nanostructure were bundled together as well as the NWs on them. It could be observed that some of the NWs appeared to be tangled (Fig. 7B). The deformation of the NWs was more drastic because the bundled bases made the NWs closer to each other so that the spacing between NWs was narrower which leads to the larger capillary force (Fig. 7C–F).

The microstructures of the interface between two touched NWs were studied using TEM. Fig. 8A and B shows typical bright field TEM images of the touched NWs. The bended NWs returned to the straight shapes, indicating that the deformation of the NWs driven by capillary was elastic deformation. The corresponding selected area electron diffraction (SAED) patterns are shown in inset. Whereas the SAED patterns in Fig. 8A indicate different orientations of the several NWs the SAED in Fig. 8B shows the only one diffraction pattern. The SAED patterns shown in the inset of Fig. 8B at the interface exhibits only two sets of well-correlated diffraction from the wurtzite ZnO [0 1 1 0] zone axis. The two sets of diffraction spots from two distinct NWs are almost overlapped with a quite small deflection angle. An HRTEM image shown in Fig. 9 was taken from the interfacial region between the touched NWs in Fig. 8B. The marked interplanar d spacing of ~0.26 nm corresponds

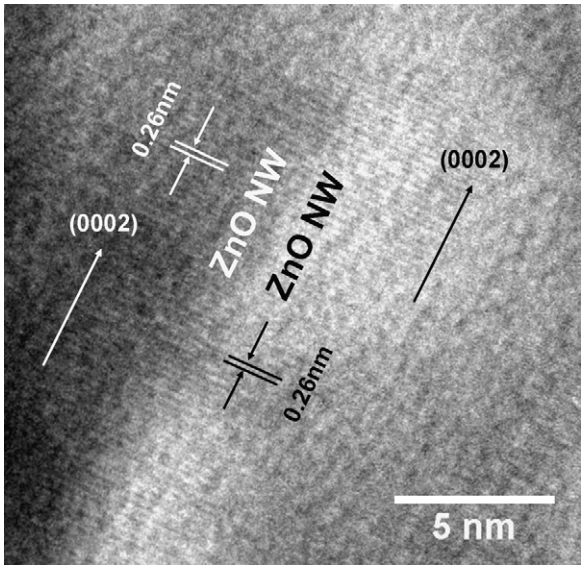

Fig. 9. HRTEM image of the interface between two touched NWs.

to that of the (0 0 0 2) lattice plane of the wurzite ZnO. It can be seen that the interfacial region is clean and uniform at the atomic scale and no amorphous intermediate layers are formed. However, some dislocations are present in the interfacial region (not shown here).

4. Summary

In summary, we have demonstrated that the original vertically aligned ZnO NW arrays can be assembled into complex micropatterns by the immersion into water or by the drip of the droplet. The fact that the morphology of ZnO NW arrays is so sensitive to liquid due to nanocarpet effect, make it clear that we could find ways to utilize the effect for developing nanostructure-based devices. The fact that the nanocarpet effect happens to the vertically aligned ZnO NW arrays may hinder many applications of ZnO NW arrays. It is also necessary to investigate the ways to resist the drawback. Therefore it is suggested to expand manipulation techniques by making use of the nanocarpet effect.

Acknowledgments

This work is supported by the Key Project of National Natural Science Foundation of China under Grant No. 50532050, the “973” program under Grant No. 2006CB604906, the Innovation Project of Chinese Academy of Sciences, the National Natural Science Foundation of China under Grant No. 60429403, No. 60506014, No. 50402016 and No. 10674133.

References

[1] C.V. Nguyen, L. Delzeit, A.M. Cassell, J. Li, J. Han, M. Meyyappan, Nano Lett. 2 (2002) 1079.
[2] K.K.S. Lau, J. Bico, K.B.K. Teo, M. Chhowalla, G.A.J. Amaratunga, W.I. Milne, G.H. McKinley, K.K. Gleason, Nano Lett. 3 (2003) 1701.
[3] N. Chakrapani, B. Wei, A. Carrillo, P.M. Ajayan, R.S. Kane, Proc. Natl. Acad. Sci. U.S.A. 101 (2004) 4009.
[4] X. Yan, B. Tay, Y. Yang, W.Y.K. Po, J. Phys. Chem. C 111 (2007) 17254.
[5] M.A. Correa-Duarte, N. Wagner, J. Rojas-Chapana, C. Morsczeck, M. Thie, M. Giersig, Nano Lett. 4 (2004) 2233.
[6] D.N. Futaba, K. Hata, T. Yamada, T. Hiraoka, Y. Hayamizu, Y. Kakudate, O. Tanaike, H. Hatori, M. Yumura, S. Iijima, Nat. Mater. 5 (2006) 987.
[7] H. Liu, S. Li, J. Zhai, H. Li, Q. Zheng, L. Jiang, D. Zhu, Angew. Chem., Int. Ed. 43 (2004) 1146.
[8] J.-G. Fan, D. Dyer, G. Zhang, Y.-P. Zhao, Nano Lett. 4 (2004) 2133.
[9] J.-G. Fan, J.-X. Fu, A. Collins, Y.-P. Zhao, Nanotechnology 19 (2008) 045713.
[10] J.-G. Fan, Y.-P. Zhao, Appl. Phys. Lett. 90 (2007) 013102.
[11] Y.-P. Zhao, J.-G. Fan, Appl. Phys. Lett. 88 (2006) 103123.
[12] M.H. Huang, S. Mao, H. Feick, H. Yan, Y. Wu, H. Kind, E. Weber, R. Russo, P. Yang, Science 292 (2001) 1897.
[13] X. Wang, J. Zhou, J. Song, J. Liu, N. Xu, Z.L. Wang, Nano Lett. 6 (2006) 2768.
[14] M.S. Arnold, P. Avouris, Z.W. Pan, Z.L. Wang, J. Phys. Chem. B 107 (2003) 659.
[15] C.J. Lee, T.J. Lee, S.C. Lyu, Y. Zhang, H. Ruh, H.J. Lee, Appl. Phys. Lett. 81 (2002) 3648.
[16] Z.L. Wang, J. Song, Science 312 (2006) 242.
[17] X. Wang, J. Song, J. Liu, Z.L. Wang, Science 316 (2007) 102.
[18] C.Q. Chen, Y. Shi, Y.S. Zhang, J. Zhu, Y.J. Yan, Phys. Rev. Lett. 96 (2006) 075505.
[19] Y. Shi, C.Q. Chen, Y.S. Zhang, J. Zhu, Y.J. Yan, Nanotechnology 18 (2007) 075709.
[20] J. Song, X. Wang, E. Riedo, Z.L. Wang, Nano Lett. 5 (2005) 1954.
[21] W.L. Hughes, Z.L. Wang, Appl. Phys. Lett. 86 (2005) 043106.
[22] C.Q. Chen, J. Zhu, Appl. Phys. Lett. 90 (2007) 043105.
[23] Y.-R. Lin, S.-S. Yang, S.-Y. Tsai, H.-C. Hsu, S.-T. Wu, I.C. Chen, Cryst. Growth Des. 6 (2006) 1951.
[24] Y. Sun, D.J. Riley, M.N.R. Ashfold, J. Phys. Chem. B 110 (2006) 15186.
[25] C. Lu, L. Qi, J. Yang, L. Tang, D. Zhang, J. Ma, Chem. Commun. 33 (2006) 3551.
[26] P. Jiang, J.-J. Zhou, H.-F. Fang, C.-Y. Wang, Z.L. Wang, S.-S. Xie, Adv. Funct. Mater. 17 (2007) 1303.
[27] Y. Sun, N.G. Ndifor-Angwafor, D.J. Riley, M.N.R. Ashfold, Chem. Phys. Lett. 431 (2006) 352.
[28] D.X. Zhao, C. Andreazza, P. Andreazza, Chem. Phys. Lett. 408 (2005) 335.
[29] F. Fang, D.X. Zhao, J.Y. Zhang, D.Z. Shen, Y.M. Lu, X.W. Fan, B.H. Li, X.H. Wang, Nanotechnology 18 (2007) 235604.
[30] X.Q. Meng, D.X. Zhao, J.Y. Zhang, D.Z. Shen, Y.M. Lu, L. Dong, Z.Y. Xiao, Y.C. Liu, X.W. Fan, Chem. Phys. Lett. 413 (2005) 450.
[31] C.H. Mastrangelo, C.H. Hsu, J. Microelectromech. Syst. 2 (1993) 33.
[32] C.H. Mastrangelo, C.H. Hsu, J. Microelectromech. Syst. 2 (1993) 44.
[33] O. Raccurt, F. Tardif, F. Arnaud d'Avitaya, T. Vareine, J. Micromech. Microeng. 14 (2004) 1083.